TP53 mutations correlate with the non-coding RNA content of small extracellular vesicles in melanoma

Maureen Labbé, Estelle Menoret, Franck Letourneur, Benjamin Saint-pierre, Laurence de Beaurepaire, Joëlle Veziers, Brigitte Dreno, Marc G Denis, Christophe Blanquart, Nicolas Boisgerault, et al.

Received: 23 March 2023 | Revised: 4 July 2023 | Accepted: 16 July 2023

DOI: 10.1002/jex2.105

RESEARCH ARTICLE

TP53 mutations correlate with the non-coding RNA content of small extracellular vesicles in melanoma

Maureen Labbé[1] | **Estelle Menoret**[1,2] | **Franck Letourneur**[3] | **Benjamin Saint-Pierre**[3] | **Laurence de Beaurepaire**[4] | **Joëlle Veziers**[5,6,7] | **Brigitte Dreno**[8] | **Marc G. Denis**[9] | **Christophe Blanquart**[1] | **Nicolas Boisgerault**[1] | **Jean-François Fonteneau**[1] | **Delphine Fradin**[1]

[1]Nantes Université, Inserm UMR 1307, CNRS UMR 6075, Université d'Angers, CRCI2NA, Nantes, France

[2]LabEx IGO "Immunotherapy, Graft, Oncology,", Nantes, France

[3]Université de Paris, Institut Cochin, INSERM, CNRS, Paris, France

[4]IECM, ONIRIS, INRAE, USC1383, Nantes, France

[5]INSERM Unit 1229, Regenerative Medicine and Skeleton, Nantes, France

[6]CHU Nantes, PHU4 OTONN, Nantes, France

[7]SC3M, SFR Santé F. Bonamy, FED 4203, UMS Inserm 016, Nantes, France

[8]Dermatology Department, Director of the Unit of Cell and Gene Therapy CHU Nantes, CIC 1413, CRCINA, University Nantes, France

[9]Department of Biochemistry, Nantes University Hospital, Nantes, France

Correspondence
Delphine Fradin, Nantes Université, Inserm UMR 1307, CNRS UMR 6075, Université d'Angers, CRCI2NA, F-44000 Nantes, France.
Email: delphine.fradin@inserm.fr

Funding information
Cancéropole Grand Ouest, Grant/Award Number: AO Structurant ExomiR; Ligue Contre le Cancer; Comités, Grant/Award Numbers: 22, 29, 35, 44 et 56; Fondation ARC pour la Recherche sur le Cancer, Grant/Award Number: 4ème année de thèse

Abstract

Non-coding RNAs (ncRNAs) are important regulators of gene expression. They are expressed not only in cells, but also in cell-derived extracellular vesicles (EVs). The mechanisms controlling their loading and sorting remain poorly understood. Here, we investigated the impact of *TP53* mutations on the non-coding RNA content of small melanoma EVs. After purification of small EVs from six different patient-derived melanoma cell lines, we characterized them by small RNA sequencing and lncRNA microarray analysis. We found that *TP53* mutations are associated with a specific micro and long non-coding RNA content in small EVs. Then, we showed that long and small non-coding RNAs enriched in *TP53* mutant small EVs share a common sequence motif, highly similar to the RNA-binding motif of Sam68, a protein interacting with hnRNP proteins. This protein thus may be an interesting partner of p53, involved in the expression and loading of the ncRNAs. To conclude, our data support the existence of cellular mechanisms associate with *TP53* mutations which control the ncRNA content of small EVs in melanoma.

KEYWORDS
long non-coding RNA, microRNA, Small extracellular vesicle, TP53 mutations

1 | BACKGROUND

Exosome are small extracellular vesicles (EVs) (50–150 nm) generated from the late endosome, also called multivesicular bodies (MVB), in a cell. The MVB then fuses with the plasma membrane leading to exosomes release. Depending on the cell origin, these small EVs can contain lipids, proteins, DNA and RNAs. Actually, large amount of RNAs has been identified inside small EVs by array profiling or next generation sequencing. RNAs has long been at the centre of molecular biology, first as a template (messenger RNA, mRNA) or as an infrastructural platform (ribosomal RNA, rRNA and transfer RNA, tRNA), and then as regulator of gene expression (non-coding RNA, ncRNA). Among this last group, a class of small ncRNAs, called microRNAs (miRNAs) has been extensively studied. miRNAs are short ncRNAs of ~22 nucleotides that mediate gene silencing. They exhibit tissue-specific expression patterns (Landgraf et al., 2007) and are epigenetically regulated (Ha & Kim, 2014). Up to now, more than 2600 mature miRNAs have been described in *Homo sapiens* and more than 60% of the mRNA can be regulated by a least one miRNA (Friedman et al., 2009). In the past decades, miRNAs have been demonstrated to be extensively dysregulated in human cancers, showing their important role in tumour onset, growth, and metastasis (Goodall et al., 2020; He et al., 2020). Another class of ncRNAs which has gain great interest in the cancer field is the long ncRNAs (lncRNAs). LncRNAs are longer than 200 nucleotides and do not encode proteins. They tend to be shorter than mRNAs, have fewer exons, lack robust translated open reading frames (ORFs) and are poorly conserved (Quinn & Chang, 2016). According to the ENCODE project, the human genome includes more than 30,000 lncRNAs and this number is constantly evolving (Tragante & Moore, 2014). LncRNAs can be classified according to their position relative to protein-coding genes (Mercer et al., 2009) such as "antisense lncRNAs", which are transcribed from the antisense strand of a protein coding gene, and which usually regulate its gene expression. Recent studies have highlighted their implication in cancer onset, progression as well as in drug resistance (Goodall et al., 2020; Jiang et al., 2019). Interestingly, like miRNAs, lncRNAs seem to be selectively packed into small EVs, such as exosomes (Gezer et al., 2014; Zhang et al., 2015), to participate in cell-to-cell communication (O'Brien et al., 2020).

Metastatic cutaneous melanoma is a highly aggressive form of skin cancer which represents a major clinical problem. Its incidence continues to rise in Western countries, and no curative treatments are available at this stage, although new treatments such as targeted therapies and immunotherapies have significantly improved patient survival (Schadendorf et al., 2015). Melanoma exhibits significantly elevated base mutation rates compared to other solid tumours (Pleasance et al., 2010), with enrichment of the cytidine to thymidine (C > T) transitions characteristic of an ultraviolet light-induced mutational signature. About 50% of melanoma patients harbour an activating *BRAF* (B-Raf proto-oncogene, serine/threonine kinase) mutation, and 15%–20% have a *NRAS* (neuroblastoma RAS viral (v-ras) oncogene homolog) mutation, with high RAS/RAF kinase activity promoting tumour growth (Forbes et al., 2006). As a major player in carcinogenesis, *TP53* (tumour protein p53) is mutated in a majority of human cancers including melanoma (Muller & Vousden, 2013), where 20% of cases carry a somatic mutation, which is not as rare as previously thought (Hodis et al., 2012; Shtivelman et al., 2014). The tumour suppressor protein p53 is considered as the "guardian of the genome". It controls many cellular processes including proliferation, death and DNA repair. Therefore, loss of its tumour suppressor function is a common feature of many cancers, and mutant p53 protein usually acquires oncogenic functions (Muller & Vousden, 2013).

RAS and *BRAF* mutations have been previously associated with a specific miRNA cargo of EVs (Cha et al., 2015; Lunavat et al., 2017; McKenzie et al., 2016). Since p53 is an important transcription factor, we hypothesized that the ncRNA populations present in small EVs derived from *TP53* mutant melanoma cells are different from those found in small EVs from *TP53* WT melanoma cells, as observed for *RAS* and *BRAF* in various cancers. Using six different melanoma cell lines established from local patients that differ in *TP53* gene mutational status, we showed that *TP53* mutated cells release small EVs containing long and small ncRNAs distinct from those of WT cells. Next, we demonstrated that the ncRNAs enriched in the mutant small EVs shared a common sequence motif, very similar to the RNA-binding motif of Sam68. Finally, we found that Sam68 protein was enriched in *TP53* mutant melanoma cell lines, which could explain a different expression profile and loading of ncRNAs in their small EVs.

2 | METHODS

2.1 | Cell lines

The melanoma cell lines M113, M117, M28, M18, M88, and M6 were established from patient's metastatic tumour fragments from the Department of Dermato-Oncology (CHU Nantes) in our Inserm Unit or in the GMP Unit of Cell therapy of Nantes and are registered in the Biocollection PC-U892-NL (CHU Nantes).

Cell lines were cultured in RPMI 1640 (Eurobio, Cat#CM1RPM00-01) supplemented with 10% exosome-depleted fetal bovine serum (Gibco, Cat#A2720801), L-glutamine (2 mM, Gibco, Cat#25030-024) and penicillin-streptomycin (100 μg/mL, Gibco, Cat#15140-122). Cell lines were tested each week for mycoplasma contamination using the PlasmoTest-Mycoplasma Detection kit (Invivogen, Cat#Rep-ptrk) according to the manufacturer's protocol. Contaminated cells were discarded. Fresh cell lines were thawed every 2 months at approximately passage 10.

2.2 | Analysis of mutational status

DNA was extracted from the cell lines using Gentra Puregene kit (Qiagen, Cat#1042606) according to the manufacturer's protocol. NGS libraries were then prepared using the QIAseq Targeted DNA Custom Panel (QIAGEN, Courtaboeuf, France) Kit, an amplicon library construction kit based on the SPE (Single primer extension) technology (https://www.qiagen.com/us/products/discovery-and-translational-research/next-generation-sequencing/dna-sequencing/somatic-panels/qiaseq-targeted-dna-custom-panels). This panel targets 20 genes (*AKT1* (v-akt murine thymoma viral oncogene homolog 1), *ALK* (anaplastic lymphoma receptor tyrosine kinase), *BRAF, CTNNB1* (catenin (cadherin-associated protein), beta 1), *EGFR* (epidermal growth factor receptor), *ERBB2* (erb-b2 receptor tyrosine kinase 2), *FGFR2* (fibroblast growth factor receptor 2), *FGFR3* (fibroblast growth factor receptor 3), *HRAS* (Harvey rat sarcoma viral oncogene homolog), *IDH1* (isocitrate dehydrogenase 1 (NADP+), soluble), *IDH2* (isocitrate dehydrogenase 2 (NADP+), mitochondrial), *KIT* (v-kit Hardy-Zuckerman 4 feline sarcoma viral oncogene homolog), *KRAS* (Kirsten rat sarcoma viral oncogene homolog), *MAP2K1* (mitogen-activated protein kinase kinase 1), *MET* (MET proto-oncogene, receptor tyrosine kinase), *NRAS, PDGFRA* (platelet-derived growth factor receptor, alpha polypeptide), *PIK3CA* (phosphatidylinositol-4,5-bisphosphate 3-kinase, catalytic subunit alpha), *RET* (ret proto-oncogene) *and TP53*). NGS libraries were prepared according to the supplier's recommendations and then sequenced on a MiSeq sequencer (Illumina, San Diego, CA, USA). NGS data were analysed with the CLC Genomics Workbench 12.0 software (QIAGEN).

2.3 | Small EV purification

Melanoma-derived small EVs were isolated from 20×10^6 tumour cells cultured in exosome-depleted media for 24 h as previously described (Vignard et al., 2019). Briefly, differential centrifugations were performed to isolate small EVs from media: 5 min at 300 g, 10 min at 2000 g, 30 min at 10,000 g and two runs at 100,000 g for 120 min. The final pellet containing the small EVs was resuspended in PBS. We used a Beckman ultracentrifuge Optima L-80XP with a SW28 rotor.

The international society for extracellular vesicles (ISEV) recommends the use of the generic term small EVs instead of exosomes (Théry et al., 2018). According to our vesicle purification method and this recommendation, in the article we will refer to our vesicles as small EVs.

2.4 | Tunable resistive pulse sensing

Small EV size and concentration distribution were quantified using Tunable Resistive Pulse Sensing (TRPS) technology with qNano instrument (IZON). All sample were diluted in PBS 0.03% Tween 20 and recorded with two different pressures on NP150 nanopore. To calibrate size and concentration, 110 nm (mode) carboxylated polystyrene beads (IZON) were used.

For each recording, at least 500 particles were counted with a minimum rate of 100 particles/min. A stretch between 45 and 47 with a voltage between 0.5 and 0.7 V were used to achieve a stable current between 135 and 145 nA.

2.5 | Western-blot

To extract and study the subcellular distribution of proteins, small EVs and cells were lysed with NE-PER Nuclear and Cytoplasmic Extraction reagents (Thermo Scientific, Cat#78833) according to manufacturer's protocol. Protein concentration was determined by BCA (Interchim, Cat#UP40840A). Proteins were denatured at 95°C for 5 min in Laemmli buffer (Biorad, Cat#1610747). Then, they were electrophoresed by SDS-PAGE and transferred onto a PVDF membrane. The membrane was blocked for 2 h at room temperature with 5% non-fat milk. The membrane was incubated with primary antibody: mouse anti-CD63 (Invitrogen Life technologies, Cat#10628D) (1 μg/mL), or mouse anti-CD81 (Invitrogen Life technologies, Cat#10630D) (1 μg/mL), or mouse anti-Alix (Biolegend, Cat#634502) (2 μg/mL), or mouse anti-calnexin (Invitrogen Life technologies, Cat#MA3-027) (4 μg/mL) or rabbit anti-Sam68 (Thermo Scientific, Cat#PA5-62364) (0.4 μg/mL)) or mouse anti-actin (Invitrogen, Cat#MA5-11869) (0.5 μg/mL) or mouse anti-Histone H3 (Active Motif, Cat#39763) (2 μg/mL) overnight at 4°C, followed by a secondary antibody ((goat anti-mouse IgG, HRP-conjugated, Interchim, Cat#115-036-072) (0.8 μg/mL) or (goat anti-rabbit IgG, HRP-conjugated, Interchim, Cat#111-035-006) (0.8 μg/mL)) for another 1 h. Blots were developed with enhanced chemiluminescent (ECL) substrate (Clarity Western ECL substrate, Biorad Cat#170-5061) and protein expression was assessed using a ChemiDocMP Imaging System (Biorad).

2.6 | Transmission electron microscopy

Small EVs were investigated by negative stain electron microscopy. Briefly, small EVs were placed for 20 min on formvar-carbon coated cooper 200 mesh grids (AGS162 Agar Scientific, UK). Small EVs were then washed with PBS and fixed with 1% glutaraldehyde (Sigma Aldrich, Cat#G5882) dissolved in PBS for 5 min. After eight washes with deionized water, samples were stained with Uranyless (Delta Microscopie, France) for 1 min. The grids were coated with a thin layer of platinum (3 nm) using a Leica EM ACE600 high vacuum sputter coater. Grids with negative-stained vesicles were observed with a GeminiSEM 300 Zeiss scanning electron microscope, equipped with a STEM detector. Observations were made at 29 keV, 7.5 μm diaphragm, working distance 4 mm.

2.7 | Total RNA extraction

Total RNAs from cells and small EVs were extracted with QIAzol reagent (Qiagen) and the miRNeasy kit (Qiagen, Cat#217084) according to the manufacturer's protocols. RNA was screened for purity and concentration in a Nanodrop-1000 spectrophotometer (Thermofisher Scientific). The Agilent 2100 Bioanalyzer (Agilent) for total RNA (RNA nanochips, Cat#5067-1511) and for small RNA (small RNA chips, Agilent, Cat#5067-1548) was used to assess the large and small RNA profiles.

2.8 | Small RNA sequencing and analysis

Small RNA libraries were prepared following the Qiaseq miRNA library prep kit protocol (Qiagen, Cat#331502), starting from 100 ng of QC controlled small RNA fraction. Libraries were then sequenced after QC control on a Nextseq 500 (Illumina) using a single Read 75 bp mode. A minimum 12 million reads were obtained for each sample. Fastq files were uploaded on the QIAGEN Online Data Analysis Centre, to align sequences to miRBase release 21 and use the UMI count to prevent PCR biases. Once each sample associated with the right group, we performed a standard DESeq2 normalization method (DESeq2's median of ratios with the DESeq function). Following the package recommendations, we used the Wald test with the contrast function and the Benjamini–Hochberg FDR control procedure to identify the differentially expressed miRNA. MiRecords and miRTarbase databases implemented in multimiR (Ru et al., 2014) were used to identify validated target genes. Then, using PathfindR (Ulgen et al., 2019), we identified the KEGG (Kyoto Encyclopedia of Genes and Genomes) pathways which involved the validated target genes.

2.9 | Long non-coding RNA arrays and analysis

Expression of lncRNAs was assessed by the manufacturer using the Human LncRNA Expression Micro-arrays V5.0 (Arraystar, Cat#AS-S-LNC-H). All experimental procedures were performed following Arraystar standard protocol. Briefly, RNA samples were amplified and transcribed into Cy3-labelled cRNA by the random primer method of Quick Amp labelling kit One-color (Agilent, Cat#5190-0442). Then, labelled cRNAs were hybridized using the Agilent Gene Expression Hybridization kit (Agilent, Cat#5188-5242), and acquired array images were analysed by the Agilent feature extraction software (Agilent Technologies). Raw signal intensities were normalized in quantile method by GeneSpring GX v12.1 (Agilent), and low intensity LncRNAs were filtered. Differentially expressed LncRNAs with statistical significance were identified through Volcano Plot filtering between two groups (Fold-change (FC) > 2, p-value < 0.05). All original microarray data were deposited in the NCBI's Gene Expression Omnibus database under the reference GSE140531.

2.10 | Predicting and analysing p53 binding sites

CiiiDER was used to predict potential p53 binding site within the differentially expressed ncRNAs (Gearing et al., 2019). All the ncRNA sequences were download form the Ensembl website and scanned.

2.11 | Sequence motif analysis

MEME (Multiple Em for Motif Eliciation) Suite 4.12.0, a web-based tool for studying sequence motifs in RNA, was used to determine a common motif to miRNAs and lncRNAs overexpressed in mutant *TP53* small EVs or in the WT ones

(Bailey et al., 2015). We applied a Markov model of order 0 to identify this motif. Tomtom was applied to compare our motif against a database of known motifs (e.g., JASPAR), to rank it, to produce an alignment for each significant match, and to give us a *p*-value and a corrected *p*-value (FDR) (Gupta et al., 2007). FIMO was used to scan sequences for motif matches (Grant et al., 2011).

2.12 | cDNA synthesis and quantitative RT-qPCR of miRNAs

miR-27b-3p. miRNAs were reverse transcribed with the Mysticq microRNA cDNA Synthesis Mix (Sigma-Aldrich, Cat#MIRRT) and quantified on a QuantStudio3 system (Applied) using the Mysticq microRNA SYBR green Ready-Mix and primers (Sigma–Aldrich, Cat#MIRRM01). Each reaction sample was run in duplicate. Small nucleolar RNA 44 (snord44) (Sigma–Aldrich, Cat#MIRCP00005) was used as internal reference gene. Primers used in these analyses were miR-27b-3p (Sigma–Aldrich, Cat#MIRAP00068).

miR-23b-3p, miR-27b-3p, miR-193b-3p, miR-369-3p, miR-577, and *miR-5582-3p*. miRNAs were reverse transcribed with miRCURY LNA RT kit (Qiagen, Cat#339340) according to the manufacturer's protocol. Quantitative PCR was performed on a QuantStudio3 system (Applied) using the miRCURY LNA SYBR Green PCR kit (Qiagen, Cat#339346) and primers. Each reaction sample was run in duplicate. Small nucleolar RNA 44 (snord44) (Qiagen, Cat#339306 – YP00203902) was used as internal reference gene. Primers used in these analyses were YP02119314 for miR-23b-3p, YP00205915 for miR-27b-3p, YP00204226 for miR-193b-3p, YP00206028 for miR-369-3p, YP00205998 for miR-577 and YP02111017 for miR-5582-3p (Qiagen, Cat#339306).

For all, melting curve analysis was performed at the end of the run to ensure specificity in the amplification. The $2^{-\Delta\Delta Ct}$ method was used to calculate relative changes in expression.

2.13 | Sam68 knock-down

M117 cells (*TP53* mutated cells) were transfected with 30 nM final of Sam68 siRNA or of scramble siRNA (Mission SiRNA Universal negative 1, Sigma Cat#SIC001) using TransiT-X2 transfection reagent (Mirus, Cat#MIR6003) according to the protocol of manufacturer. Cells were plated in a T75 flask at a density of 4.2 M cells/flask and 24 h after seeding, siRNA molecules were added. The Sam68 siRNA target sequence was 5′-GCUCUUAUGGCCCAUGCCA-3′. Following 24 h of transfection, western-blot analysis was carried out to confirm the Sam68 gene knockdown as well as RT-qPCR.

2.14 | RT-qPCR

Total RNA was reverse transcribed using M-MLV reverse transcriptase (Thermo Scientific, Cat#28025013) and the RT product was used for expression analysis using Maxima SYBR Green/ROX qPCR Master Mix (Thermo Scientific, Cat#K0223). *Sam68* was amplified using the following primers: 5′-ATGAGAGACAAAGCCAAGGAGG-3′/5′-A TCACATGGGGGTCCAAAGAC-3′. *RPLP0* (Ribosomal Protein Lateral Stalk Subunit P0, 5′-GTGATGTGCAGCTGATCAAGACT-3′/5′-GATGACC AGCCCAAAGGAGA-3′) gene was used as reference genes. Each reaction sample was run in duplicate. To circumvent any issue of non-specific amplification melting curve analysis was performed with a temperature gradient of 70–95°C. The $2^{-\Delta\Delta Ct}$ method was used to calculate relative changes in expression.

2.15 | Co-immunoprecipitation

For pull down of endogenous Sam68 complexes, M117 cells (50 mg per condition) were lysed in lysis buffer according to the manufacturer's protocols (Invitrogen, Dynabeads Co-immunoprecipitation kit, Cat#14321D). One milligram of Dynabeads were coupled with IgG (Invitrogen, Cat#31325) or Sam68 antibody (Thermofisher, Cat#A302111A) at 37°C overnight. Antibody-coupled beads were subsequently incubated with cell lysate at 4°C for 30 min. Then the bound proteins were eluted and used for Western blot analysis and miRNA analysis as previously described.

2.16 | Statistical analysis

Error bars indicate ± SEM (Standard error of the mean) between biological replicates. Statistical significance was calculated by nonparametric Wilcoxon test or t test when applicable. NS, nonsignificant; $*p < 0.05$, $**p < 0.01$, $***p < 0.001$. All statistical analyses were performed with R4.0.3.

TABLE 1 Mutational status of the melanoma patient cell lines.

Patient	Sex	TP53	Consequence of the TP53 mutation*	NRAS	BRAF	Type of cancer
M113	M			Q61R		Melanoma
M28	F				V600E	Melanoma
M6	F			Q61R		Melanoma
M117	F	C277F	Loss of function	Q61H		Melanoma
M18	F	P27S	Reduced transcriptional activity		V600E	Melanoma
M88	M	C176Y	Impaired transcriptional activity		V600E	Melanoma

*according https://ckb.jax.org/gene/show?geneId=7157 or Fischer N. "The functional and clinical consequences of TP53 mutations in cancers" 2019.

3 | RESULTS

3.1 | Small EVs derived from *TP53* WT or mutated melanoma cell lines exhibit typical vesicular features

To characterize the small EVs secreted by melanoma cell lines according to their *TP53* mutational status, we first cultured melanoma cells in exosome-depleted medium at 90% confluence. Twenty-four hours later, supernatants were collected and the small extracellular vesicles were purified by ultracentrifugation. To observe the morphology of the isolated small EVs, we first performed transmission electron microscopy (TEM) analysis (Figure 1a). We confirmed that the purified particles possess a circular morphology with an intact membrane based on negative staining. Using TRPS technology, we found that the melanoma vesicles have sizes comparable to those assessed by electron microscopy, and in the typical range of small EV range (Figure 1b). Moreover, WT melanoma cells appear to produce less EVs than *TP53* mutated cells, although this is not significant.

We next examined the presence of exosome marker proteins in our isolated small EVs by western blot analysis (Figure 1c). Our results show that CD63, CD81 and Alix were enriched in our purifications. The absence of calnexin, a cytoplasmic marker (Théry et al., 2018), in our vesicle preparations compared with cell lysate samples confirms the presence of purified small EVs with minimal cytoplasmic contaminants in our preparations.

Together, our results show that our protocol efficiently purifies small EVs from melanoma cell lines.

3.2 | Small RNA profiling of melanoma small EVs from *TP53* mutant and WT cells

First, to determine whether *TP53* mutations can influence the small RNA content of melanoma small EVs, we conducted a small RNA sequencing on vesicles derived from six melanoma cell lines with distinct genotypes (Table 1). All *TP53* mutations lead to a mutant p53 protein that is unable to transactivate its target genes, resulting in the loss of its tumour suppressor functions (Fischer, 2019). However, it is also known that most of mutant p53s acquire novel oncogenic functions that could induce the expression of specific RNAs (Pitolli et al., 2019; Sabapathy, 2015; Shetzer et al., 2016). We identified 223 differentially expressed small RNAs between small EVs derived from *TP53* WT cells and mutant cells (Figure 2a, Table S1), including 118 miRNAs overexpressed in the mutants. After correction for multiple testing, five miRNAs remained significantly overexpressed in small EV from *TP53*-mutated cells compared to those from *TP53* WT cells, and three miRNAs were underrepresented (Table 2). The highest fold changes were detected for hsa-miR-5692b and hsa-miR-6508-3p, both of which were overexpressed in small EVs derived from *TP53* WT melanoma cells ($\log_2$FC = 6.25 and 6.34, respectively), whereas the most significant difference was found for hsa-miR-577 overexpressed in mutant *TP53* melanoma cell lines (adjusted p-value = 0.00133). Using mirTarbase (Huang et al., 2022) and miRecords (Xiao et al., 2009) implemented in R (multimiR package), we identified 1888 experimentally validated target genes of our five significantly overexpressed miRNAs in mutant *TP53* small EVs (Table S2). Pathway analyses showed that they are mainly enriched in the Cell cycle pathway, the Adherens junction pathway and in the Cellular senescence pathway (Figure 2b, Table S3). Regarding the three significantly under-expressed miRNAs in mutant *TP53* small EVs, we found that they could regulate the expression of 496 target genes involved in numerous signalling pathways, including the Ras signalling pathway or the Erb signalling pathway (Figure 2c, Table S4).

Interestingly, there is no difference in the small RNA content of small EV derived from *BRAF* or *NRAS* mutated melanoma cells, excepted for hsa-miR-155-5p but with discrepancies inside the *NRAS* mutated group (Figures 2d, e).

Our small RNA sequencing also highlighted the presence of piwi-interacting RNAs (piR) in melanoma small EVs, with again a different expression pattern according to the *TP53* mutational status (Figure 2a, Table 1).

Taken together, our results suggest that small EVs secreted by mutant *TP53* cancer cell lines carry a specific cargo of small RNAs.

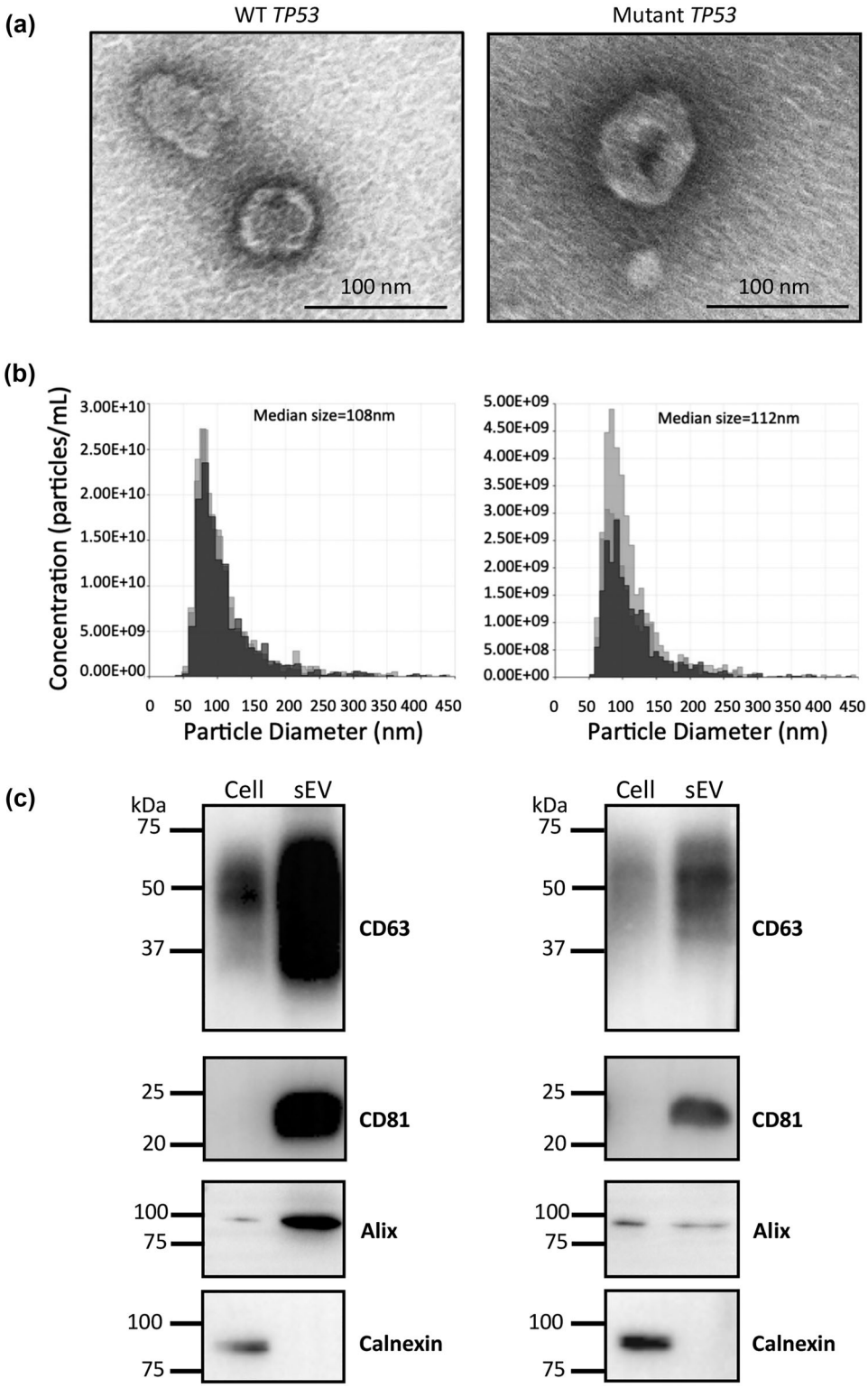

FIGURE 1 Examples of characterization of small EVs purified from a WT *TP53* cell line (M113) and a mutant *TP53* cell line (M117). (a) Representative transmission electron microscopy (TEM) images of melanoma-derived small EVs. Circular morphology and the absence of internal staining indicate intact, compartmentalized vesicles. (b) Size distributions of the three independent small EV purifications/productions by cell line by qNano technology. Size is consistent with results from TEM. (c) Protein characteristics of small EVs using western blotting technique. For consistency of comparison between small EVs and cells, 3 μg of sample was loaded per well for western blotting. $^{***}p < 0.001$.

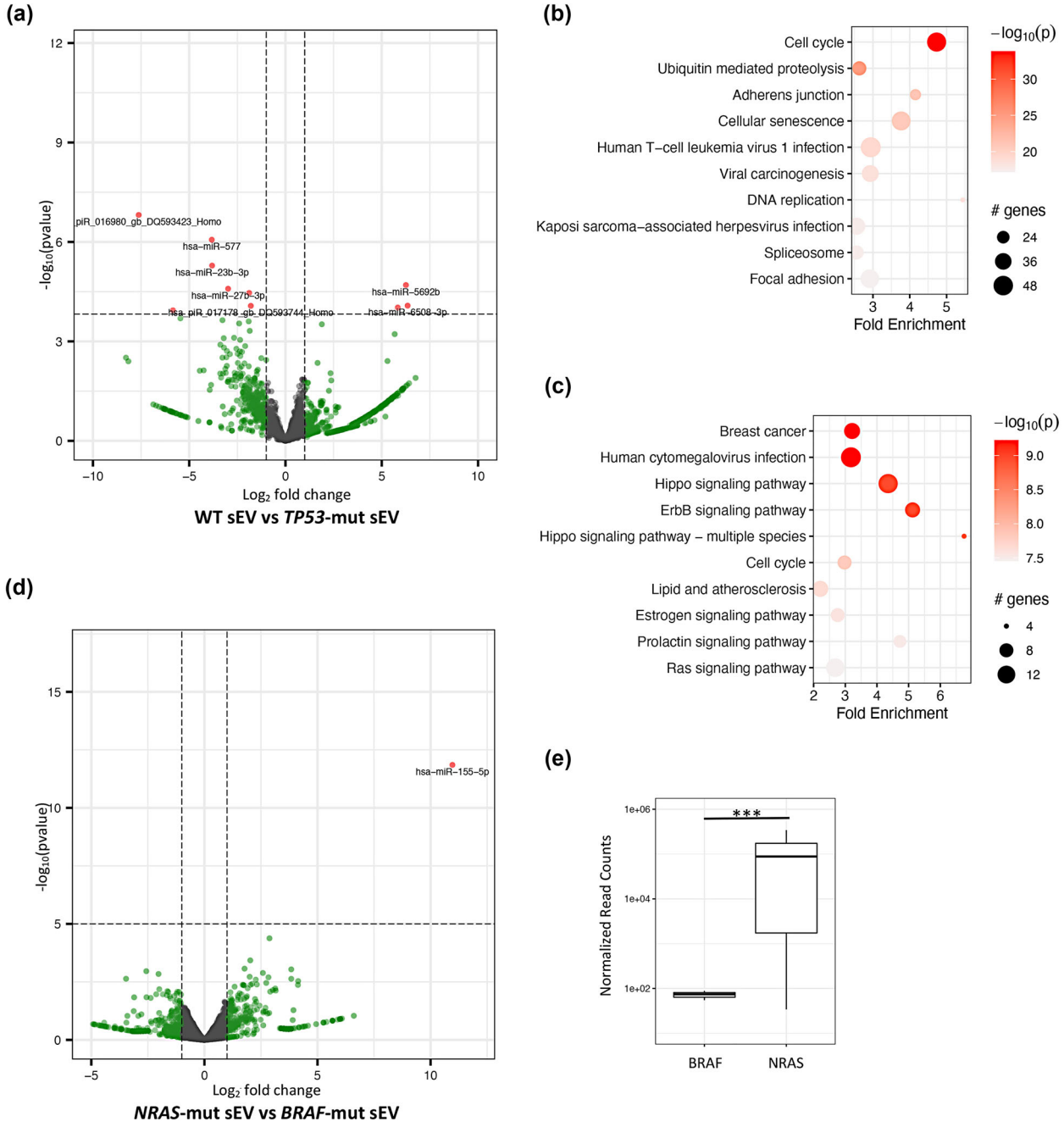

FIGURE 2 Differential miRNA content of small EVs from *TP53*-mutated or WT melanoma cells. (a) Volcano plot of adjusted *p* value as a function of weighted fold-change for small RNA (adjusted *p* value < 0.05). Red dots on the left represent significantly downregulated small RNAs in small EVs from *TP53* WT melanoma cells and on the right the upregulated ones compared to small EVs from mutant *TP53*melanoma cells. In green, miRNAs with a log2 fold change >2 or −2. (b) Enrichment analysis of the 1888 targets of the significantly enriched miRNAs in small EVs derived from *TP53* mutant cells. (c) Enrichment analysis of the 496 targets of the significantly enriched miRNAs in small EVs derived from *TP53* WT cells. (d) Volcano plot of differentially expressed small RNA between small EVs from *NRAS* or *BRAF* mutated melanoma cell lines. (e) Expression level of hsa-miR-155-5p in small EVs from *NRAS* and *BRAF* mutated melanoma cells. $^{*}p < 0.05$, $^{**}p < 0.01$, $^{***}p < 0.001$.

3.3 | Small EV-derived from *TP53* mutated cell lines have a specific lncRNA cargo

Next, we performed a lncRNA profiling assay using the Human V5.0 LncRNA array (ArrayStar), which contained 33,045 lncRNAs to evaluate the influence of *TP53* mutations on their expression in small EVs. We found that 1046 lncRNAs were differentially expressed between *TP53* mutant and WT small EVs ($p < 0.05$, Table S5). After correction for multiple testing (FDR < 0.05), 10 lncRNAs remained significantly overexpressed in the mutants, and 46 were downregulated (Table 3). The highest fold change was

TABLE 2 Small RNAs differentially expressed between *TP53* WT and mutated derived small EVs after correction for multiple testing.

Small RNA name	log2FC	Regulation	*p*-value	Adjusted *p*-value
hsa-miR-5692b	−6.256	Up in WT	2.01e−05	0.01546
hsa-miR-6508-3p	−6.342	Up in WT	8.35e−05	0.03261
hsa-miR-5582-3p	−5.832	Up in WT	9.53e−05	0.03264
hsa_piR_016980_gb_DQ593423_Homo	7.625	Up in mutant	1.53e−07	0.00047
hsa-miR-577	3.827	Up in mutant	8.61e−07	0.00133
hsa-miR-23b-3p	3.811	Up in mutant	5.17e−06	0.00532
hsa-miR-27b-3p	2.979	Up in mutant	2.58e−05	0.01595
hsa-miR-193b-3p	1.886	Up in mutant	3.45e−05	0.01774
hsa_piR_017178_gb_DQ593744_Homo	1.799	Up in mutant	8.46e−05	0.03262
hsa-miR-369-3p	5.844	Up in mutant	0.00011	0.03558

Abbreviation: FC, fold change.

detected for *LINC01531*, which was overexpressed in small EVs derived from *TP53* WT melanoma cells (FC = 18.4), whereas the most significant difference was found for *G065582* which was also overexpressed in small EVs derived from *TP53* WT melanoma cell lines.

We also compared the lncRNA content of small EVs derived from *BRAF*-mutated cells to small EVs derived from *NRAS*-mutated cells. To avoid the effect of *TP53* mutations, we first analysed small EVs from M28 versus those from M113 and M6 cell lines (Table 1). Few significant differences were observed and none remained significant after correction for multiple testing except *G014584* and *G087573* (FDR = 0.046, FC = 2.12 and FC = 2.27, respectively) (Figure S1). Interestingly, we identified 915 lncRNAs differentially expressed between small EVs derived from M28 and M117 melanoma cell lines, probably explained again by *TP53* mutations (Table S6). Indeed, 16 remained significant after correction for multiple testing, and half of which had been identified in our analysis according to the *TP53* mutational status.

Overall, our results suggest that *TP53* mutations also modulate the lncRNA content of melanoma-derived small EVs.

3.4 | *TP53* does not directly regulate expression of the differentially expressed ncRNA

To decipher the mechanisms underlying these differences, we first postulated that p53, as a transcriptional factor, could directly regulate the expression of these ncRNAs. Using Ciiider, we predicted and analysed the putative promoter regions (−1500 bases upstream to +500 bases downstream of the transcriptional Start Site (TSS)) of the referenced ncRNAs. We found that no differentially expressed miRNAs or lncRNAs between small EVs derived from WT and *TP53* mutated melanoma cells has a p53 binding site (Figure S2). Based on this result, we postulated that a protein other than p53 might be involved in the differential expression of these ncRNAs in small melanoma EVs.

To shed light on this protein, we performed an unbiased sequence motif search using the MEME suite and found a common and conserved "AUMAAADW" motif (Figure 3a top, Figure S3A) among the ncRNAs (long and small) enriched in small EVs derived from *TP53* mutant cells. Only four of the 46 lncRNAs significantly overexpressed in WT ones displayed this motif and no miRNAs (Figure S3B), all of which encompassed a different motif (Figure S3C).

To identify the RNA Binding Proteins (RBP) that might interact with the "AUMAAADW" motif, we compared it to known motifs from JASPAR using Tomtom. We found a strong match with the RNA-binding motif of KHDRBS1 (KH RNA Binding Domain Containing, Signal Transduction Associated 1) protein, also called Sam68 ($p = 4.10^{-4}$, FDR = 0.046, Figure 3a bottom).

Next, we quantified Sam68 expression in melanoma cell lines by western blot analysis to see whether this protein was uniformly expressed in *TP53* WT and mutated cells. We found that Sam68 was significantly overexpressed in *TP53* mutated melanoma cells compared to *TP53* WT cells ($p < 0.05$, Figure 3b). Sam68 is a multifunctional player involved in RNA splicing in the nucleus, and RNA trafficking in the cytoplasm. To go further, we then investigated its expression in these different compartments. We found that Sam68 is mainly localized in the nucleus of *TP53* mutant cells, while it is concentrated in the cytoplasm of *TP53* WT cells, and is never found in small EV (Figure 3c).

To further establish the relationship between Sam68 and the overexpressed miRNAs in *TP53* mutant small EVs, we first measured their expression in the parental melanoma cells by RT-qPCR. We found that hsa-miR-23b-3p, hsa-miR-27b-3p, hsa-miR193b-3p and hsa-miR-577 were significantly upregulated in *TP53* mutant melanoma cells compared to the WT ones as observed in their small EVs. (Figure 4a). hsa-miR-369-3p showed the same trend and not hsa-miR-5582-3p as expected. We conclude that the miRNA cargo of the small EVs reflects the miRNA content of the cell and that overexpression of Sam68 in *TP53*-mutated cells could explain the increased expression of these miRNAs in mutated cells and in their small EVs.

TABLE 3 LncRNAs differentially expressed between small EVs derived from *TP53* WT and mutated cell lines after correction for multiple testing.

Seqname	Gene symbol	Probe name	*p*-value	FDR	FC	Regulation	RNA length	Chrom	Start	End
ENST00000524011	RP11-567J20.2	ASHGV40049258	0.00005	0.024	−1.66	Up in WT	764	chr8	49464574	49469001
NR_027374	LHFPL3-AS2	ASHGV40046916	0.00005	0.024	−1.56	Up in WT	1911	chr7	104535074	104567092
NR_103785	SIX3-AS1	ASHGV40026680	0.00004	0.024	−5.41	Up in WT	1000	chr2	45167292	45168646
T327275	G076664	ASHGV40046702	0.00001	0.024	−4.42	Up in WT	931	chr7	77412554	77422526
TCONS_00016111	XLOC_007499	ASHGV40053254	0.00004	0.024	−1.89	Up in WT	838	chr9	107854175	107881755
T361327	G085356	ASHGV40051912	0.00001	0.024	−7.79	Up in WT	3329	chr9	87846883	87901869
uc.328-	uc.328	ASHGV40060346	0.00001	0.024	−3.60	Up in WT	231	chr11	31825662	31825893
T269110	G062330	ASHGV40037841	0.00003	0.024	−2.21	Up in WT	872	chr4	106507921	106509384
T045400	G010525	ASHGV40005915	0.00001	0.024	−2.71	Up in WT	1544	chr10	86891653	86908209
T280442	G065193	ASHGV40040065	0.00001	0.024	−8.00	Up in WT	2416	chr5	31073203	31079151
ENST00000520370	RP11-246K15.1	ASHGV40050700	0.00000	0.024	−10.8	Up in WT	567	chr8	58405442	58458502
T103832	G024479	ASHGV40014961	0.00002	0.024	−3.53	Up in WT	7142	chr14	48395227	48425786
NR_047501	LINC00572	ASHGV40012404	0.00004	0.024	−4.35	Up in WT	575	chr13	30492783	30500788
ENST00000589715	RP11-95O2.1	ASHGV40022684	0.00004	0.024	−5.70	Up in WT	2124	chr18	34814081	34816205
T174516	G040475	ASHGV40024317	0.00005	0.024	−1.72	Up in WT	858	chr19	37493514	37495877
T253632	G058432	ASHGV40035176	0.00003	0.024	−2.87	Up in WT	484	chr3	161253382	161259349
T281807	G065582	ASHGV40041690	0.00000	0.024	−5.94	Up in WT	8282	chr5	43708823	43717951
T310559	G072798	ASHGV40044029	0.00003	0.024	−6.07	Up in WT	2828	chr6	121289933	121321536
T150828	G034969	ASHGV40021968	0.00003	0.024	−3.19	Up in WT	632	chr17	52018999	52020662
ENST00000433388	RP1-137D17.1	ASHGV40044436	0.00002	0.024	−2.91	Up in WT	588	chr6	169770092	169788480
TCONS_00001475	XLOC_000801	ASHGV40005850	0.00005	0.024	−6.22	Up in WT	1005	chr1	41430712	41432244
ENST00000501075	RP5-940J5.6	ASHGV40010971	0.00005	0.025	−11.0	Up in WT	2196	chr12	6687787	6693905
T289006	G067586	ASHGV40042317	0.00006	0.025	−4.21	Up in WT	2266	chr5	132378114	132386100
uc021yja.1	AK309215	ASHGV40041260	0.00007	0.027	−4.87	Up in WT	1250	chr5	178046291	178047541
T283696	G066125	ASHGV40040337	0.00008	0.030	−1.44	Up in WT	9045	chr5	68463861	68472906
GSE61474_TCONS_00086259	GSE61474_XLOC_016271	ASHGV40013180	0.00010	0.032	−1.64	Up in WT	640	chr13	32870858	32873037
T265433	G061336	ASHGV40037557	0.00011	0.035	−3.57	Up in WT	6246	chr4	63377813	63387499
NR_040046	LINC01531	ASHGV40003944	0.00011	0.035	−18.4	Up in WT	3312	chr19	35896508	35907742
NR_040586	STAG3L4	ASHGV40003962	0.00012	0.036	−2.14	Up in WT	2143	chr7	66767624	66786513

(Continues)

TABLE 3 (Continued)

Seqname	Gene symbol	Probe name	*p*-value	FDR	FC	Regulation	RNA length	Chrom	Start	End
ENST00000532553	CTD-2530H12.8	ASHGV40007363	0.00013	0.038	−11.1	Up in WT	546	chr11	75307188	75308315
T239530	G055089	ASHGV40035733	0.00014	0.039	−7.14	Up in WT	4862	chr3	28373404	28378266
NR_040090	CYP21A1P	ASHGV40044889	0.00014	0.039	−2.06	Up in WT	2429	chr6	31973412	31976686
T077001	G017807	ASHGV40058142	0.00016	0.042	−1.29	Up in WT	1330	chr12	42174705	42326603
ENST00000570945	RP11-65J21.3	ASHGV40018723	0.00017	0.042	−3.27	Up in WT	651	chr16	14396144	14420210
NR_120530	LOC101928443	ASHGV40007287	0.00016	0.042	−10.0	Up in WT	548	chr11	69902335	69910030
ENST00000606398	RP11-301G7.1	ASHGV40049198	0.00016	0.042	−1.36	Up in WT	594	chr8	40377083	40377677
T280390	G065173	ASHGV40057089	0.00018	0.044	−8.19	Up in WT	1409	chr5	30197842	30207116
T226978	G052410	ASHGV40032326	0.00019	0.044	−1.62	Up in WT	2609	chr21	44160879	44163488
T200813	G046374	ASHGV40058520	0.00019	0.044	−4.31	Up in WT	2238	chr2	150444411	150705024
ENST00000429821	Z83001.1	ASHGV40000687	0.00021	0.046	−6.38	Up in WT	577	chr11	31658874	31789501
T375146	G088543	ASHGV40054999	0.00021	0.046	−5.29	Up in WT	8498	chrX	54200516	54209142
T278798	G064688	ASHGV40039926	0.00020	0.046	−3.17	Up in WT	3420	chr5	9591958	9601206
T048874	G011415	ASHGV40004938	0.00022	0.047	−6.21	Up in WT	2037	chr10	115469835	115472270
T356527	G084106	ASHGV40052701	0.00024	0.049	−3.47	Up in WT	3544	chr9	22126890	22301706
ENST00000366376	RP13-259N13.2	ASHGV40005507	0.00025	0.049	−5.90	Up in WT	452	chr10	33973682	33975992
ENST00000593107	RP11-264B14.2	ASHGV40002579	0.00024	0.049	−1.60	Up in WT	247	chr17	59147216	59147717
TCONS_00017209	XLOC_008025	ASHGV40055211	0.00004	0.024	2.08	Up in mutant	435	chrX	100671834	100672797
ENST00000454439	RP1-102D24.5	ASHGV40033267	0.00003	0.024	1.87	Up in mutant	545	chr22	45831743	45844624
T013727	G003008	ASHGV40033280	0.00002	0.024	2.01	Up in mutant	11333	chr1	79954319	79967235
TCONS_00010119	XLOC_004585	ASHGV40059402	0.00004	0.024	1.75	Up in mutant	403	chr5	141615465	141616011
TCONS_00027618	XLOC_013142	ASHGV40059793	0.00007	0.027	1.59	Up in mutant	665	chr19	53727161	53727903
T292580	G068453	ASHGV40042674	0.00007	0.029	1.83	Up in mutant	457	chr5	163680433	163681040
NR_123721	PKD1P6	ASHGV40004687	0.00009	0.031	2.25	Up in mutant	5208	chr16	15198158	15230816
TCONS_00014980	XLOC_007059	ASHGV40049179	0.00009	0.032	1.41	Up in mutant	1173	chr8	38721755	38725271
T039485	G009045	ASHGV40058014	0.00017	0.042	1.55	Up in mutant	1797	chr10	32239015	32242583
ENST00000441907	RP11-446F3.2	ASHGV40000938	0.00025	0.049	2.48	Up in mutant	764	chr10	2488446	2489546

Note: *p*-value were calculated from unpaired T-test and FDR (False discovery Rate) from Benjamin Hochberg.
Abbreviations: Chrom, chromosome; FC, fold change; FDR, false discovery rate; Seqname: sequence name.

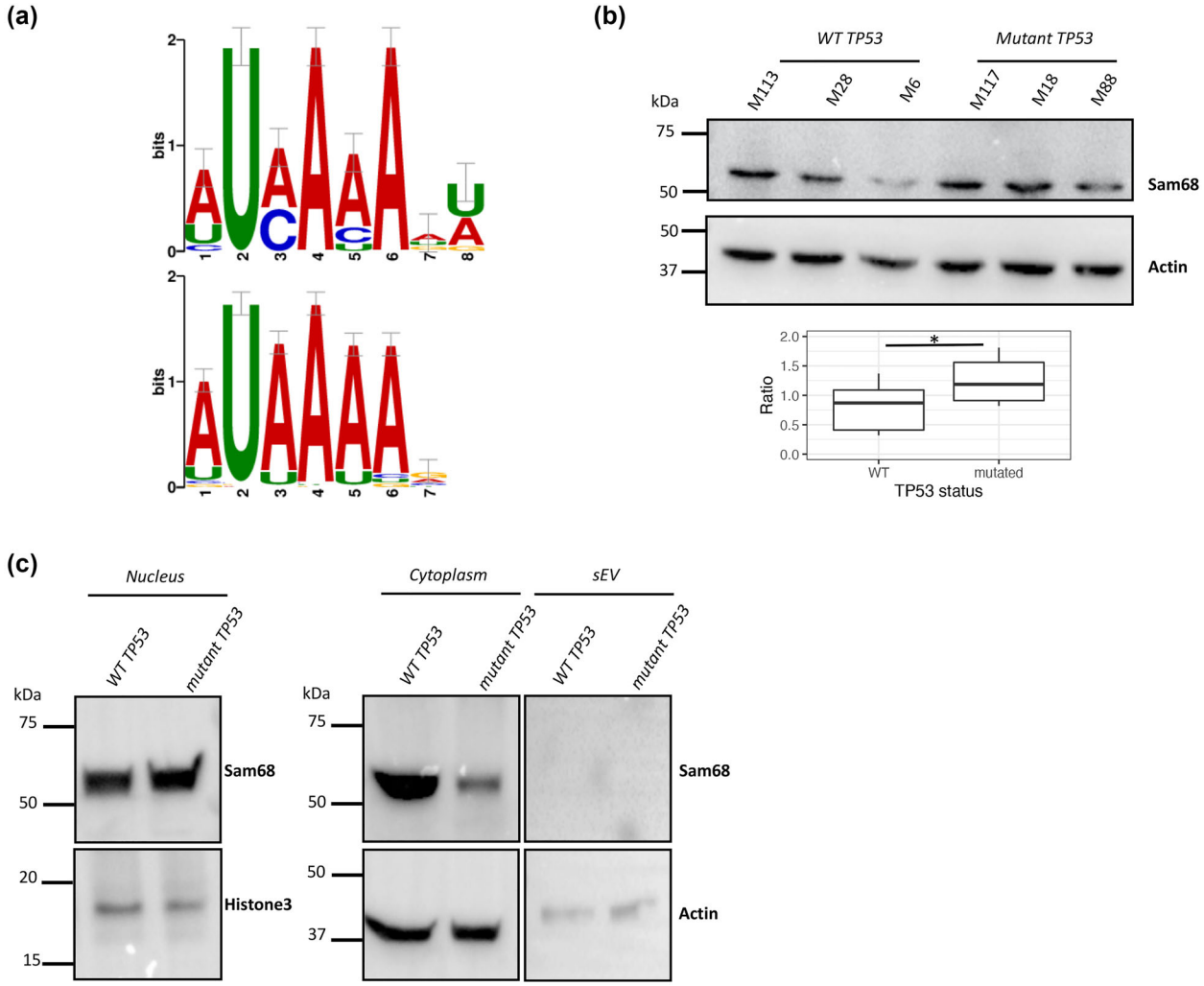

FIGURE 3 Sam68 is overexpressed in the nucleus of mutant *TP53* melanoma cell lines to regulate RNA expression. (a) 8-mer motif enriched in RNA overexpressed in mutant *TP53* small EVs. On the top, RNA motif found in our enriched RNA according to MEME. On the bottom, the RNA-binding motif of KHDRBS1 protein (Sam68) found through Tomtom analysis. (b) Quantification of Sam68 expression and differences between *TP53* WT and *TP53* mutant melanoma cells by western blot analysis. The optical density of each sample was measured and normalized using a housekeeping protein (Actin) run on the same gel using ImageJ. Data are expressed as relative expression (ratio Sam68/Actin), $n = 3$. (c) Measurement of Sam68 expression in the cytoplasm, the nucleus and the small EVs of *TP53* mutant (M117) and WT (M113) melanoma cell lines by western blot analysis. Normalization of the Sam68 protein input was performed using the actin protein in the cytoplasm and in small EVs and using the Histone 3 protein in the nucleus. $^*p < 0.05$.

In addition, when Sam68 expression was reduced by a siRNA-mediated knock-down (KD) (Figure 4b, c), we observed a slight decrease in hsa-miR-23b-3p, hsa-miR-27b-3p, hsa-miR193b-3p, hsa-miR-369-3p and hsa-miR-577 in KD Sam68 *TP53*-mutated melanoma cells, and, to a greater extend, in their small EVs (Figure 4d). This suggests that Sam68 regulates, at least in part, their expression and maybe more importantly their loading in melanoma derived small EVs.

Finally, to decipher whether these miRNAs directly interact with Sam68, we immunoprecipitated Sam68 from *TP53* mutant cells (Figure 4e) and conducted PCR analyses. We detected hsa-miR-23b-3p, hsa-miR-27b-3p and hsa-miR193b-3p but not hsa-miR-5582-3p as expected since it did not encompass the Sam68 motif (Figure 4f). We also detected hsa-miR-369-3p and hsa-miR-577 at a lower intensity.

In conclusion, Sam68 seems to be involve in the differential ncRNA cargo of *TP53* mutant small EVs from melanoma cells through direct interaction with some of them.

4 | DISCUSSION

Secretion and reciprocal exchange of small EVs between cells is an important step in cell-cell communication, especially in the tumour microenvironment. Small EVs are particularly enriched in non-coding RNAs which upon uptake by recipient cells can regulate gene expression and play a critical role. In this study, we showed that the *TP53* mutational status of cells was associated

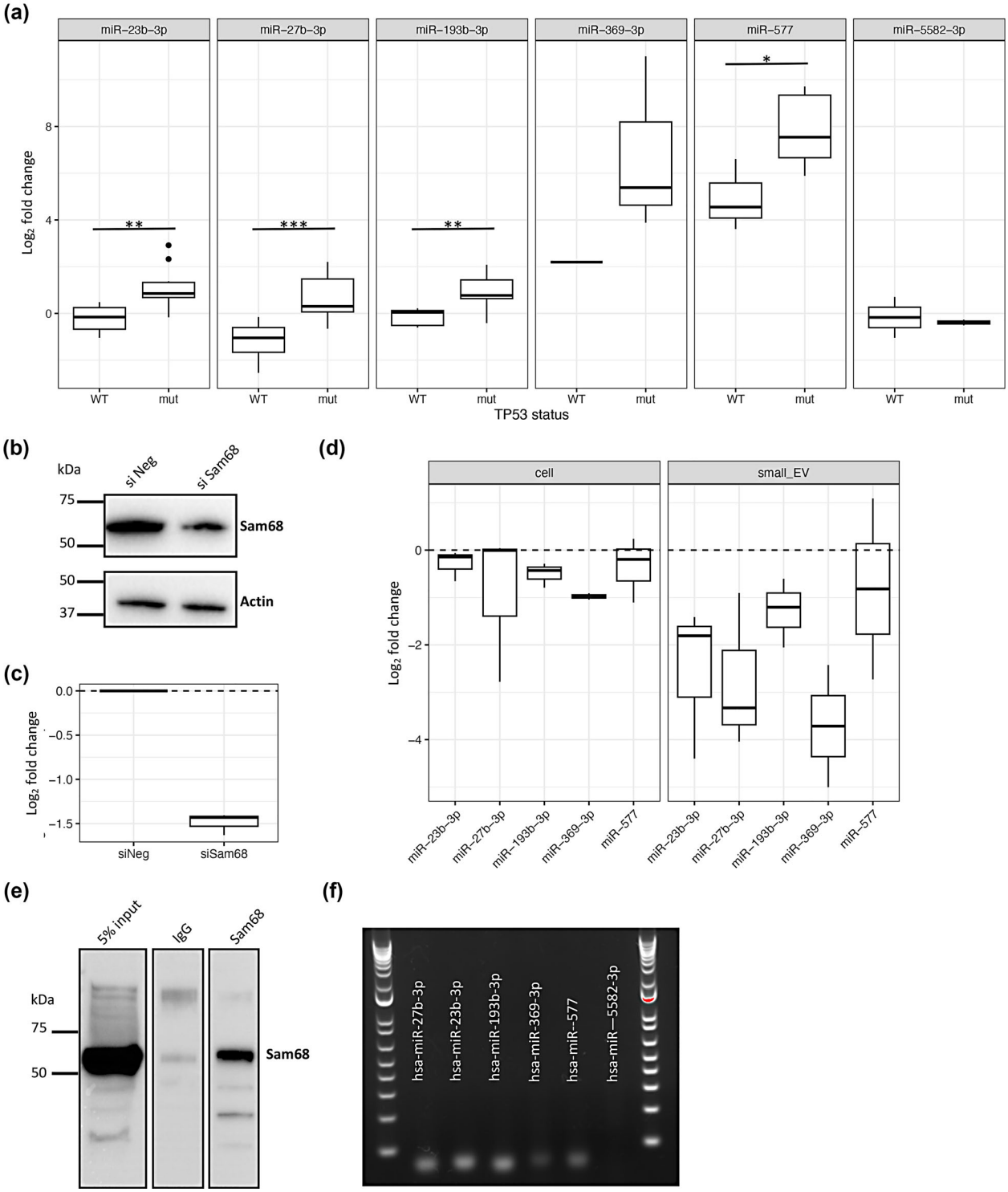

FIGURE 4 Intronic miRNA expressions are correlated with Sam68 expression in *TP53* mutated melanoma patients from TCGA. (a) Expression in melanoma cells lines of the miRNAs overexpressed in *TP53* mutant small EVs and of one downregulated (hsamiR- 5582-3p) (WT: M113, M28, M6 and mut: M117, M18, M88), $n = 3$. (b) Sam68 expression level in *TP53* mutated cell line M117 after transfection with a siRNA targeting Sam68 or with a scramble siRNA (si Neg). Normalization of the Sam68 protein input was performed using the actin protein. (c) Relative Sam68 mRNA expression was determined by qPCR after normalization with the RPLP0 housekeeping gene, $n = 3$ (d) Expression of our candidate miRNAs overexpressed in *TP53* mutant small EVs in M117 cells transfected with Sam68 siRNA compared to siNeg, $n = 3$. (e) Western blot probed with anti-Sam68 antibody to assess Sam68 associated with the captured beads following Sam68 immunoprecipitation compared to control IgG immunoprecipitated and total Input. (f) PCR analysis of candidate miRNAs following immunoprecipitation of Sam68. $^{*}p < 0.05$, $^{**}p < 0.01$, $^{***}p < 0.001$.

with a specific ncRNA cargo of their small EVs in melanoma. Current knowledge on the impact of *TP53* on small EVs is limited to its effect on the endosomal compartment of the cell and on the production of small EVs (Lespagnol et al., 2008; Yu et al., 2006, 2009), but nothing is known about its impact on their RNA content, although this has already been described for *BRAF* mutants under vemurafenib treatment, for example (Lunavat et al., 2017).

RNA loading into small EVs is not fully understood, but it appears to be driven by specific sequences interacting with various proteins (Santangelo et al., 2016; Vignard et al., 2019; Villarroya-Beltri et al., 2013, 2014; Wozniak et al., 2020), or dependent on genetic mutations (Cooks et al., 2018; Lunavat et al., 2017; McKenzie et al., 2016). Indeed, we found that some mutations that lead to loss-of-function or reduced function of p53 conduct to a specific pattern of expression of ncRNAs in the cell and in their small EVs. This could be the consequence of a higher expression of Sam68 in the mutant cells than in the WT cells. This protein, also known as KHDRBS1, was found in the nucleus and in cytoplasm of both melanoma cell types, but appeared enriched in the nucleus of *TP53*-mutated cells and, conversely, enriched in the cytoplasm of the WT cells. Sam68 in the nucleus, can be involved in numerous steps of RNA processing, form transcription to alternative splicing, to nuclear export, and in the cytoplasm, it takes part to signalling complexes and associates with RNA trafficking and loading into vesicles (Bielli et al., 2011). Indeed, Cloutier *et al.* showed that Sam68 interacted with hnRNP A1/A2 proteins, which are previously described in the loading of specific miRNA into exosomes (Villarroya-Beltri et al., 2013). Our data point in both directions since we showed that miRNAs enriched in *TP53* mutant small EVs were also more highly expressed in the cell. We therefore postulate that these miRNAs, all derived from intronic regions of messenger RNAs (except hsa-miR-369-3p) could be more spliced in mutant cells than in *TP53* WT cells, leading not only to their overexpression but also to greater loading of them in small EVs. Indeed, we found that knockdown of Sam68 in mutant cells led to a larger decrease in hsa-miR-23b-3p, hsa-mir-27b-3p, hsa-miR-193b-3p, hsa-miR-369-3p and hsa-mir-577 in small EVs than in their parental cells. However, the exact relationship between p53, Sam68 and miRNAs remains to be elucidated.

Our small RNA sequencing also identified enriched piwi-interacting RNA (piRNA) in small EVs. piRNAs can be divided into three groups based on their origins (mRNA, transposon-derived or ncRNA) (Lin, 2007). They are small non-coding RNAs that regulate transposon and gene expression through various processes. They can cleave mRNA directly or recruit histone or DNA methyltransferases to induce histone modifications and DNA methylation (Iwasaki et al., 2015). Aberrant expressions of piRNAs and Piwi proteins have been frequently reported in different cancers (Liu et al., 2019; Martinez et al., 2015), but so far have not been observed in human melanoma. Interestingly, circulating piR have been described as promising biomarkers for gastric cancer (Ameli Mojarad et al., 2022), colorectal cancer (Qu et al., 2019; Tosar et al., 2021), prostate cancer (Peng et al., 2021) and so on (Zhou et al., 2023). piRNAs have several advantages as biomarkers. First, their number (~20–30,000) far exceeds the number of miRNAs (at least 10 times more than miRNAs), they are stable in many body fluids and can be easily purified from urine, serum, and EVs. However, many challenges remain, including how precisely quantify piRNAs or how distinguish real piRNA to fragment of other coding or non-coding RNAs.

Our data support the hypothesis that long RNAs export as well in small EVs. It remains unknown whether there is a strict RNA size limitation for inclusion into them; however, the mean size in small vesicles seems to be about 200 nucleotides (O'Brien et al., 2020). One limitation of our study is the use of a microarray to investigate lncRNAs, so we cannot rule out that the lncRNAs loaded into our small EVs are not of full-length.

Although the biological relevance of these findings remains to be determined, we found that miRNAs enriched in mutant small EVs compared to WT small EVs target genes involved mainly in cell cycle. Cell cycle dysregulation is a classic feature of cancer cells as they divide continuously and excessively. But tight control of the cell cycle is also important in potential recipient cells located in the tumour microenvironment. For example, activated T cells must proliferate rapidly to engage an efficient response against tumour cells (Hiam-Galvez et al., 2021). The functional role of most lncRNA remains to be discovered, making the effect of their transfer by small EVs on recipient cells less straightforward, as well as the potential impact of their disappearance in cells. However, one of them, *LHFPL3-AS2* was previously described in lung cancer where low expression levels have been associated with a poor overall survival, making it a potentially useful prognostic biomarker (Cheng et al., 2022).

A last limitation of our study is the heterogeneity of the TP53 mutations that we have investigated. Even if all conduct to a loss or a reduce protein function, generated mutants can have different oncogenic functions according to their mutations.

In summary, our study catalogued the presence of different types of ncRNAs in small EVs from melanoma cells lines mutated or not mutated for *TP53*. Further investigation is required to validate the function of these different ncRNA on recipient cells.

AUTHOR CONTRIBUTIONS

Maureen Labbé, Estelle Menoret and Delphine Fradin performed experiments. Delphine Fradin conceived and designed the study. Laurence de Beaurepaire performed TRPS experiments, Joëlle Veziers the electron microscopy experiments, Marc G. Denis the genomic sequencing experiments and analysis, and Franck Letourneur performed the small RNA sequencing. Brigitte Dreno, Christophe Blanquart, Nicolas Boisgerault and Jean-François Fonteneau provided samples and cell lines. Maureen Labbé, Benjamin Saint-Pierre and Delphine Fradin performed array and RNA sequencing data analysis. Delphine Fradin wrote the manuscript. All authors reviewed and edited the manuscript.

ACKNOWLEDGEMENTS

The authors thank all the members of the genomic facility "GENOM'IC" (Institut Cochin Paris) for their expert technical assistance. This work was supported by grants from "Ligue contre le cancer—Comités 22, 29, 35, 44 et 56″" and from "Cancéropole Grand Ouest—AO Structurant—ExomiR". Maureen Labbé is supported by the ARC Fundation. This work was realized in the context of the LabEX IGO program supported by the National Research Agency via the investment of the future program ANR-11-LABX-0016-01″.

CONFLICT OF INTEREST STATEMENT

The authors declare no competing interests.

ORCID

Maureen Labbé https://orcid.org/0000-0002-1495-4150
Delphine Fradin https://orcid.org/0000-0001-6231-2649

REFERENCES

Ameli Mojarad, M., Ameli Mojarad, M., Shojaee, B., & Nazemalhosseini-Mojarad, E. (2022). piRNA: A promising biomarker in early detection of gastrointestinal cancer. *Pathology - Research and Practice*, *230*, 153757.

Bailey, T. L., Johnson, J., Grant, C. E., & Noble, W. S. (2015). The MEME suite. *Nucleic Acids Research*, *43*, W39–49.

Bielli, P., Busà, R., Paronetto, M. P., & Sette, C. (2011). The RNA-binding protein Sam68 is a multifunctional player in human cancer. *Endocrine-Related Cancer*, *18*, R91–102.

Cha, D. J., Franklin, J. L., Dou, Y., Liu, Q., Higginbotham, J. N., Beckler, M. D., Weaver, A. M., Vickers, K., Prasad, N., Levy, S., Zhang, B., Coffey, R. J., & Patton, J. G. (2015). KRAS-dependent sorting of miRNA to exosomes. *Elife*, *4*, e07197.

Cheng, Z., Lu, C., Wang, H., Wang, N., Cui, S., Yu, C., Wang, C., Zuo, Q., Wang, S., Lv, Y., Yao, M., Jiang, L., & Qin, W. (2022). Long noncoding RNA LHFPL3-AS2 suppresses metastasis of non-small cell lung cancer by interacting with SFPQ to regulate TXNIP expression. *Cancer Letters*, *531*, 1–13.

Cooks, T., Pateras, I. S., Jenkins, L. M., Patel, K. M., Robles, A. I., Morris, J., Forshew, T., Appella, E., Gorgoulis, V. G., & Harris, C. C. (2018). Mutant p53 cance-rs reprogram macrophages to tumor supporting macrophages via exosomal miR-1246. *Nature Communications*, *9*, 771.

Fischer, N. (2019). *The functional and clinical consequences of TP53 mutations in cancer*. University of Toronto.

Forbes, S., Clements, J., Dawson, E., Bamford, S., Webb, T., Dogan, A., Flanagan, A., Teague, J., Wooster, R., Futreal, P. A., & Stratton, M. R. (2006). Cosmic 2005. *British Journal of Cancer*, *94*, 318–322.

Friedman, R. C., Farh, K. K., Burge, C. B., & Bartel, D. P. (2009). Most mammalian mRNAs are conserved targets of microRNAs. *Genome Research*, *19*, 92–105.

Gearing, L. J., Cumming, H. E., Chapman, R., Finkel, A. M., Woodhouse, I. B., Luu, K., Gould, J. A., Forster, S. C., & Hertzog, P. J. (2019). CiiiDER: A tool for predicting and analysing transcription factor binding sites. *PLoS ONE*, *14*, e0215495.

Gezer, U., Özgür, E., Cetinkaya, M., Isin, M., & Dalay, N. (2014). Long non-coding RNAs with low expression levels in cells are enriched in secreted exosomes. *Cell Biology International*, *38*, 1076–1079.

Goodall, G. J., & Wickramasinghe, V. O. (2020). RNA in cancer. *Nature Reviews Cancer*, *21*(1), 22–36. https://doi.org/10.1038/s41568-020-00306-0

Grant, C. E., Bailey, T. L., & Noble, W. S. (2011). FIMO: Scanning for occurrences of a given motif. *Bioinformatics*, *27*, 1017–1018.

Gupta, S., Stamatoyannopoulos, J. A., Bailey, T. L., & Noble, W. S. (2007). Quantifying similarity between motifs. *Genome Biology*, *8*, R24.

Ha, M., & Kim, V. N. (2014). Regulation of microRNA biogenesis. *Nature Reviews Molecular Cell Biology*, *15*, 509–524.

He, B., Zhao, Z., Cai, Q., Zhang, Y., Zhang, P., Shi, S., Xie, H., Peng, X., Yin, W., Tao, Y., & Wang, X. (2020). miRNA-based biomarkers, therapies, and resistance in Cancer. *International Journal of Biological Science*, *16*, 2628–2647.

Hiam-Galvez, K. J., Allen, B. M., & Spitzer, M. H. (2021). Systemic immunity in cancer. *Nature Reviews Cancer*, *21*, 345–359.

Hodis, E., Watson, I. R., Kryukov, G. V., Arold, S. T., Imielinski, M., Theurillat, J.-P., Nickerson, E., Auclair, D., Li, L., Place, C., DiCara, D., Ramos, A. H., Lawrence, M. S., Cibulskis, K., Sivachenko, A., Voet, D., Saksena, G., Stransky, N., Onofrio, R. C., & Chin, L. (2012). A landscape of driver mutations in melanoma. *Cell*, *150*, 251–263.

Huang, H.-Y., Lin, Y.-C.-D., Cui, S., Huang, Y., Tang, Y., Xu, J., Bao, J., Li, Y., Wen, J., Zuo, H., Wang, W., Li, J., Ni, J., Ruan, Y., Li, L., Chen, Y., Xie, Y., Zhu, Z., Cai, X., … Huang, H. (2022). miRTarBase update 2022: An informative resource for experimentally validated miRNA–target interactions. *Nucleic Acids Research*, *50*, D222–30.

Iwasaki, Y. W., Siomi, M. C., & Siomi, H. (2015). PIWI-interacting RNA: Its biogenesis and functions. *Annual Review of Biochemistry*, *84*, 405–433.

Jiang, M.-C., Ni, J.-J., Cui, W.-Y., Wang, B.-Y., & Zhuo, W. (2019). Emerging roles of lncRNA in cancer and therapeutic opportunities. *American Journal of Cancer Research*, *9*, 1354–1366.

Landgraf, P., Rusu, M., Sheridan, R., Sewer, A., Iovino, N., Aravin, A., Pfeffer, S., Rice, A., Kamphorst, A. O., Landthaler, M., Lin, C., Socci, N. D., Hermida, L., Fulci, V., Chiaretti, S., Foà, R., Schliwka, J., Fuchs, U., Novosel, A., … Tuschl, T. (2007). A mammalian microRNA expression atlas based on small RNA library sequencing. *Cell*, *129*, 1401–1414.

Lespagnol, A., Duflaut, D., Beekman, C., Blanc, L., Fiucci, G., Marine, J.-C., Vidal, M., Amson, R., & Telerman, A. (2008). Exosome secretion, including the DNA damage-induced p53-dependent secretory pathway, is severely compromised in TSAP6/Steap3-null mice. *Cell Death & Differentiation*, *15*, 1723–1733.

Lin, H. (2007). piRNAs in the germ line. *Science*, *316*, 397–397.

Liu, Y., Dou, M., Song, X., Dong, Y., Liu, S., Liu, H., Tao, J., Li, W., Yin, X., & Xu, W. (2019). The emerging role of the piRNA/piwi complex in cancer. *Molecular Cancer*, *18*, 123.

Lunavat, T. R., Cheng, L., Einarsdottir, B. O., Bagge, R. O., Muralidharan, S. V., Sharples, R. A., Lässer, C., Gho, Y. S., Hill, A. F., Nilsson, J. A., & Lötvall, J. (2017). BRAFV600 inhibition alters the microRNA cargo in the vesicular secretome of malignant melanoma cells. *PNAS*, *114*, E5930–9.

Martinez, V. D., Vucic, E. A., Thu, K. L., Hubaux, R., Enfield, K. S. S., Pikor, L. A., Becker-Santos, D. D., Brown, C. J., Lam, S., & Lam, W. L. (2015). Unique somatic and malignant expression patterns implicate PIWI-interacting RNAs in cancer-type specific biology. *Scientific Reports*, *5*, 10423.

McKenzie, A. J., Hoshino, D., Hong, N. H., Cha, D. J., Franklin, J. L., Coffey, R. J., Patton, J. G., & Weaver, A. M. (2016). KRAS-MEK signaling controls Ago2 sorting into exosomes. *Cell Reports*, *15*, 978–987.

Mercer, T. R., Dinger, M. E., & Mattick, J. S. (2009). Long non-coding RNAs: Insights into functions. *Nature Reviews Genetics*, *10*, 155–159.

Muller, P. A. J., & Vousden, K. H. (2013). p53 mutations in cancer. *Nature Cell Biology*, *15*, 2–8.
O'Brien, K., Breyne, K., Ughetto, S., Laurent, L. C., & Breakefield, X. O. (2020). RNA delivery by extracellular vesicles in mammalian cells and its applications. *Nature Reviews Molecular Cell Biology*, *21*, 585–606.
O'Brien, K., Breyne, K., Ughetto, S., Laurent, L. C., & Breakefield, X. O. (2020). RNA delivery by extracellular vesicles in mammalian cells and its applications. *Nature Reviews Molecular Cell Biology*, *21*, 585–606.
Peng, Q., Chiu, P. K.-F., Wong, C. Y.-P., Cheng, C. K.-L., Teoh, J. Y.-C., & Ng, C.-F. (2021). Identification of piRNA targets in urinary extracellular vesicles for the diagnosis of prostate cancer. *Diagnostics (Basel)*, *11*, 1828.
Pitolli, C., Wang, Y., Mancini, M., Shi, Y., Melino, G., & Amelio, I. (2019). Do mutations turn p53 into an oncogene? *International Journal of Molecular Sciences*, *20*, 6241.
Pleasance, E. D., Cheetham, R. K., Stephens, P. J., McBride, D. J., Humphray, S. J., Greenman, C. D., Varela, I., Lin, M., Ordóñez, G. R., Bignell, G. R., Ye, K., Alipaz, J., Bauer, M. J., Beare, D., Butler, A., Carter, R. J., Chen, L., Cox, A. J., Edkins, S., … Stratton, M. R. (2010). A comprehensive catalogue of somatic mutations from a human cancer genome. *Nature*, *463*, 191–196.
Qu, A., Wang, W., Yang, Y., Zhang, X., Dong, Y., Zheng, G., Wu, Q., Zou, M., Du, L., Wang, Y., & Wang, C. (2019). A serum piRNA signature as promising non-invasive diagnostic and prognostic biomarkers for colorectal cancer. *CMAR*, *11*, 3703–3720.
Quinn, J. J., & Chang, H. Y. (2016). Unique features of long non-coding RNA biogenesis and function. *Nature Reviews Genetics*, *17*, 47–62.
Ru, Y., Kechris, K. J., Tabakoff, B., Hoffman, P., Radcliffe, R. A., Bowler, R., Mahaffey, S., Rossi, S., Calin, G. A., Bemis, L., & Theodorescu, D. (2014). The multiMiR R package and database: Integration of microRNA–target interactions along with their disease and drug associations. *Nucleic Acids Research*, *42*, e133.
Sabapathy, K. (2015). The contrived mutant p53 oncogene – beyond loss of functions. *Frontiers in Oncology*, *5*, 276.
Santangelo, L., Giurato, G., Cicchini, C., Montaldo, C., Mancone, C., Tarallo, R., Battistelli, C., Alonzi, T., Weisz, A., & Tripodi, M. (2016). The RNA-binding protein SYNCRIP is a component of the hepatocyte exosomal machinery controlling microRNA sorting. *Cell Reports*, *17*, 799–808.
Schadendorf, D., Fisher, D. E., Garbe, C., Gershenwald, J. E., Grob, J.-J., Halpern, A., Herlyn, M., Marchetti, M. A., McArthur, G., Ribas, A., Roesch, A., & Hauschild, A. (2015). Melanoma. *Nature Reviews Disease Primers*, *1*, 15003.
Shetzer, Y., Molchadsky, A., & Rotter, V. (2016). Oncogenic mutant p53 gain of function nourishes the vicious cycle of tumor development and cancer stem-cell formation. *Cold Spring Harbor Perspectives in Medicine*, *6*, a026203.
Shtivelman, E., Davies, M. Q. A., Hwu, P., Yang, J., Lotem, M., Oren, M., Flaherty, K. T., & Fisher, D. E. (2014). Pathways and therapeutic targets in melanoma. *Oncotarget*, *5*, 1701–1752.
Théry, C., Witwer, K. W., Aikawa, E., Alcaraz, M. J., Anderson, J. D., Andriantsitohaina, R., Antoniou, A., Arab, T., Archer, F., Atkin-Smith, G. K., Ayre, D. C., Bach, M., Bachurski, D., Baharvand, H., Balaj, L., Baldacchino, S., Bauer, N. N., Baxter, A. A., Bebawy, M., … Zuba-Surma, E. K. (2018). Minimal information for studies of extracellular vesicles 2018 (MISEV2018): A position statement of the International Society for Extracellular Vesicles and update of the MISEV2014 guidelines. *Journal of Extracellular Vesicles*, *7*, 1535750.
Tosar, J. P., García-Silva, M. R., & Cayota, A. (2021). Circulating SNORD57 rather than piR-54265 is a promising biomarker for colorectal cancer: Common pitfalls in the study of somatic piRNAs in cancer. *Rna*, *27*, 403–410.
Tragante, V., & Moore, J. H. (2014). Asselbergs FW. The ENCODE Project and Perspectives on Pathways. *Genetic Epidemiology*, *38*, 275–280.
Ulgen, E., Ozisik, O., & Sezerman, O. U. (2019). pathfindR: An R package for comprehensive identification of enriched pathways in omics data through active subnetworks. *Frontiers in Genetics*, *10*, 858.
Vignard, V., Labbé, M., Marec, N., André-Grégoire, G., Jouand, N., Fonteneau, J.-F., Labarrière, N., & Fradin, D. (2019). MicroRNAs in tumor exosomes drive immune escape in melanoma. *Cancer Immunology Research*, *8*(2), 255–267. https://doi.org/10.1158/2326-6066.CIR-19-0522
Villarroya-Beltri, C., Baixauli, F., Gutierrez-Vazquez, C., Sanchez-Madrid, F., & Mittelbrunn, M. (2014). Sorting it out: Regulation of exosome loading. *Seminars in Cancer Biology*, *28*, 3–13.
Villarroya-Beltri, C., Gutierrez-Vazquez, C., Sanchez-Cabo, F., Perez-Hernandez, D., Vazquez, J., Martin-Cofreces, N., Martinez-Herrera, D. J., Pascual-Montano, A., Mittelbrunn, M., & Sánchez-Madrid, F. (2013). Sumoylated hnRNPA2B1 controls the sorting of miRNAs into exosomes through binding to specific motifs. *Nature Communications*, *4*, 2980.
Wozniak, A. L., Adams, A., King, K. E., Dunn, W., Christenson, L. K., Hung, W.-T., & Weinman, S. A. (2020). The RNA binding protein FMR1 controls selective exosomal miRNA cargo loading during inflammation. *Journal of Cell Biology*, *219*(10), e201912074.
Xiao, F., Zuo, Z., Cai, G., Kang, S., Gao, X., & Li, T. (2009). miRecords: An integrated resource for microRNA-target interactions. *Nucleic Acids Research*, *37*(Database issue), D105–110.
Yu, X., Harris, S. L., & Levine, A. J. (2006). The regulation of exosome secretion: A novel function of the p53 protein. *Cancer Research*, *66*, 4795–4801.
Yu, X., Riley, T., & Levine, A. J. (2009). The regulation of the endosomal compartment by p53 the tumor suppressor gene. *The FEBS Journal*, *276*, 2201–2212.
Zhang, J., Li, S., Li, L., Li, M., Guo, C., Yao, J., & Mi, S. (2015). Exosome and exosomal microRNA: Trafficking, sorting, and function. *Genomics, Proteomics & Bioinformatics*, *13*, 17–24.
Zhou, J., Xie, H., Liu, J., Huang, R., Xiang, Y., Tian, D., & Bian, E. (2023). PIWI-interacting RNAs: Critical roles and therapeutic targets in cancer. *Cancer Letters*, *562*, 216189.

SUPPORTING INFORMATION

Additional supporting information can be found online in the Supporting Information section at the end of this article.

How to cite this article: Labbé, M., Menoret, E., Letourneur, F., Saint-Pierre, B., de Beaurepaire, L., Veziers, J., Dreno, B., Denis, M. G., Blanquart, C., Boisgerault, N., Fonteneau, J.-F., & Fradin, D. (2023). *TP53* mutations correlate with the non-coding RNA content of small extracellular vesicles in melanoma. *Journal of Extracellular Biology*, *2,* e105. https://doi.org/10.1002/jex2.105